al 1–4% of the scattered events. Since the maximum correction for nuclear absorption was 40%, ignoring neutrals amounted to, at most, a 2% error.

[35]The collision length for steel which we used was 9.6 cm. This was obtained from an unpublished experimental report by K. Stanfield, who calculated the total cross sections by means of an optical model, using a Woods-Saxon potential for the distribution of matter in the nucleus. These results were in reasonable agreement with the data for nuclei of high atomic number given in Ref. 24.

[36]B. Rossi, *High Energy Particles* (Prentice-Hall, Englewood Cliffs, New Jersey, 1952), p. 81, Eq. (13).

[37]Ref. 36, p. 82, Fig. 2.19.1.

[38]Ref. 36, p. 51, Fig. 2.11.2.

[39]H. A. Bethe, W. Heitler, Proc. R. Soc. Lond. A146, 63 (1934).

[40]See Ref. 36, p. 53, Eq. (19), and p. 83. Eq. (16).

PHYSICAL REVIEW D VOLUME 9, NUMBER 5 1 MARCH 1974

Production of f^0 mesons in 4.5-GeV/c $\pi^- p$ interactions*

L. E. Holloway, B. Huld,† M. Jordan,‡ U. Koetz,§ U. E. Kruse, D. W. Mortara,‖ and L. J. Nodulman
University of Illinois at Urbana, Illinois 61801

S. Bernstein, S. Margulies, and D. W. McLeod
University of Illinois at Chicago Circle, Chicago, Illinois 60680
(Received 23 July 1973)

An optical spark chamber and neutron time-of-flight spectrometer experiment studied the reaction $\pi^- p \to \pi^+\pi^- n$ at incident pion momentum of 4.5 GeV/c in the mass region of the f^0 meson. Analysis of the data shows no evidence for anomalous structure in the f^0 mass spectrum. The two-pion differential cross section in the f^0 region is consistent with Wolf's one-pion-exchange model for momentum transfers (squared) $-t \lesssim 0.7$ (GeV/c)^2. The differential cross section is larger than that predicted at high momentum transfer, and may be attributed to natural-parity-exchange contributions as evidenced in the f^0 decay distribution.

I. INTRODUCTION

There has been considerable controversy and conflicting experimental data on the existence of a split structure for the A_2 meson. Contradictory reports of possible structure in the f^0 mass spectrum have also been published.[1] The A_2 and f^0 mesons belong to the same ($J^P = 2^+$) SU(3) nonet, and may be expected to exhibit similar characteristics.

Production of f^0 mesons has been reasonably well studied at low momentum transfer[2]; however, the data have been statistically limited for momentum transfers squared beyond $|t| \sim 0.6$ (GeV/c)^2. The decay angular distribution is fairly well characterized by one-pion-exchange (OPE) production with some interference from an s-wave dipion state. The differential cross section $d\sigma/dt$ for f^0 production has been well described by OPE with absorption, or by Wolf's one-pion-exchange model.[3]

We report here results of a neutron-counter time-of-flight/optical spark chamber experiment studying the reaction $\pi^- p \to \pi^+\pi^- n$ at 4.5 GeV/c incident π^- momentum. Features of the spectrometer include high missing-mass resolution and uniform acceptance for f^0 production over a broad range of momentum transfer, $0.125 < |t| < 1.6$ (GeV/c)^2.

We find no evidence for splitting of the f^0 mass spectrum. We also find that f^0 production at high momentum transfer [$|t| > 0.7$ (GeV/c)^2] is more copious than expected from an OPE model and is characterized by natural parity exchange.

II. EXPERIMENTAL DETAILS

The experiment was performed in the 17° beam of the Argonne ZGS. Figure 1 shows the apparatus surrounding the 30-cm liquid hydrogen target. A larger view showing the neutron flight path is provided in Fig. 2. The apparatus was similar to that of a previous experiment studying the ω meson.[4] However, in order to improve mass resolution several changes were made. The essential differences were as follows:

1. A fifteen-element scintillation hodoscope (M) was placed at the first (momentum dispersed) focus of the beam.

2. The horizontal displacement and angle of the incident pion was measured by two multiwire proportional counters (MWPC) placed one meter apart in front of the hydrogen target. Each consisted of 20 wires spaced 2 mm apart.[5] The momentum hodoscope and MWPC information determined the

incident beam pion momentum to $\delta p/p = 0.2\%$ rms.

3. The 13×4 array of neutron counters was placed 20 meters from the target. Each counter consisted of an 11-cm-wide×25-cm-high×30-cm-long block of NE102 scintillator viewed by a 58 AVP photomultiplier. The counters were separated (spaced) horizontally by a gap of two counter widths so that a set of three positions was needed to cover a range of angles completely. The range subtended by a set of positions was about half the total angular range of 34.45° to 57.55°. In addition to two extreme sets of positions which together covered the entire range, central angles were covered by a third set of positions. This overlap served as a potential check that any fine structure observed in the mass spectrum in the Jacabian peak region did not result from counter malfunction.

4. A twenty-four-element hodoscope (Pi) was placed downstream of the liquid hydrogen target. The counters were horizontal strips. The strip at beam height was divided into two counters, one on either side of the beam. The central five strips were 2.54 cm high and the remaining outer strips were 3.18 cm high. All were 0.64 cm thick and 68.58 cm long.

5. A thin-foil optical spark chamber, constructed of aluminum foil and polyurethane foam,[6] was used. This chamber presented negligible mass to neutron flight paths. The chamber consisted of three groups of four gaps, each having an 87-cm-square active area. This square was displaced 15.9 cm to the beam's right. Along the beam line the gaps were deadened by Mylar patches. The chambers were photographed in 90° stereo. The two mirrors viewing the top of the thin foil chamber were set at a relative stereo angle of 40 mrad in order to help resolve track pairing ambiguities.

6. All plates in the shower chambers were 0.32-cm-thick stainless steel, forming a total of seven radiation lengths. Further details of the apparatus can be found in Refs. 4 and 7.

While accumulating data, the number of hits in the M and Pi hodoscope counters, neutron counters, and MWPCs were monitored by an on-line Xerox Data Systems Σ-2 computer. In addition, total singles rates for the M hodoscope, the Pi hodoscope, and the neutron counters were monitored. The magnetic field of the second bending magnet was monitored continuously with an NMR probe. Time-of-flight calibration was monitored by simultaneous accumulation of prompt (γ) and data events. Neutron counter threshold settings were checked in separate pulse height runs. A grid of additional fiducial marks on the optical spark chambers was illuminated every thousandth frame.

The electronic signature of an incident beam particle can be expressed

$$\text{BEAM} = M \cdot B1 \cdot B2 \cdot \overline{H}A \cdot \overline{P},$$

where M is a logical OR of the momentum hodoscope and $\overline{P}$ is a pileup veto rejecting beam particle occurring within 20 ns either before or after

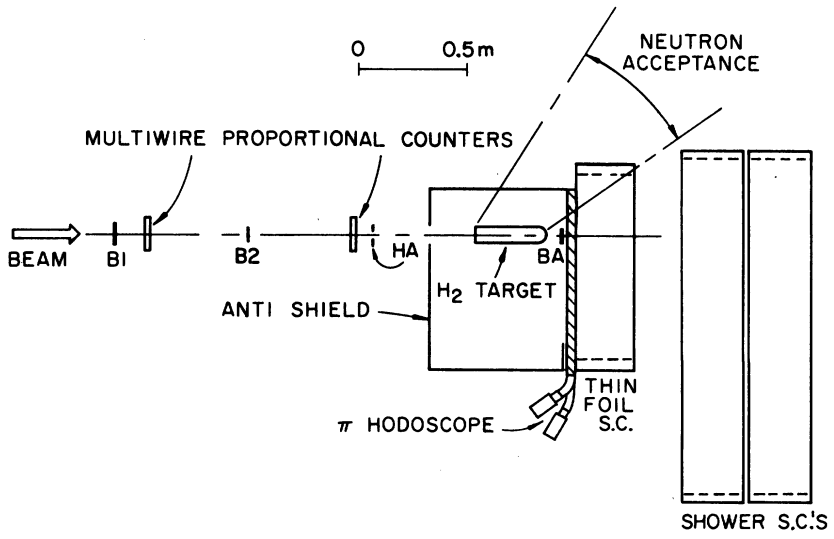

FIG. 1. Target area. The counters $B1$, $B2$, and HA served to define the beam electronically. The absence of a signal in the counter BA signalled an interaction. Large scintillation counters in a box surrounding the target on five sides formed the "antishield" (AS) which vetoed interactions resulting in charged particles at large angles. The presence of two charged particles entering the thin-foil chamber was signalled by the Pi hodoscope. The beam and the emerging charged tracks are measured by multiwire proportional counters and optical spark chambers, respectively.

another beam particle. No Cherenkov requirement was used; previously, a freon gas Cherenkov counter was employed to measure electron and muon contamination of the beam (0.8% and 0.5%, respectively) and was removed thereafter.

The electronic signature of an event was

$$\text{EVENT} = \text{BEAM} \cdot \overline{BA} \cdot 2\pi \cdot \overline{AS} \cdot \overline{SCA} \cdot N,$$

where 2π represents two and only two counts in the Pi hodoscope. Counters placed around the target generated the signal AS when charged particles were produced at wide angles to the beam. The anticoincidence counters SCA vetoed events in which secondary interactions in the downstream spark chamber could produce a spurious neutron signal. A neutron-counter signal in an appropriately delayed time interval formed N. A separate neutron signal, set to include the prompt peak, was used for prompt events. The allowed region of mass and momentum transfer, determined by

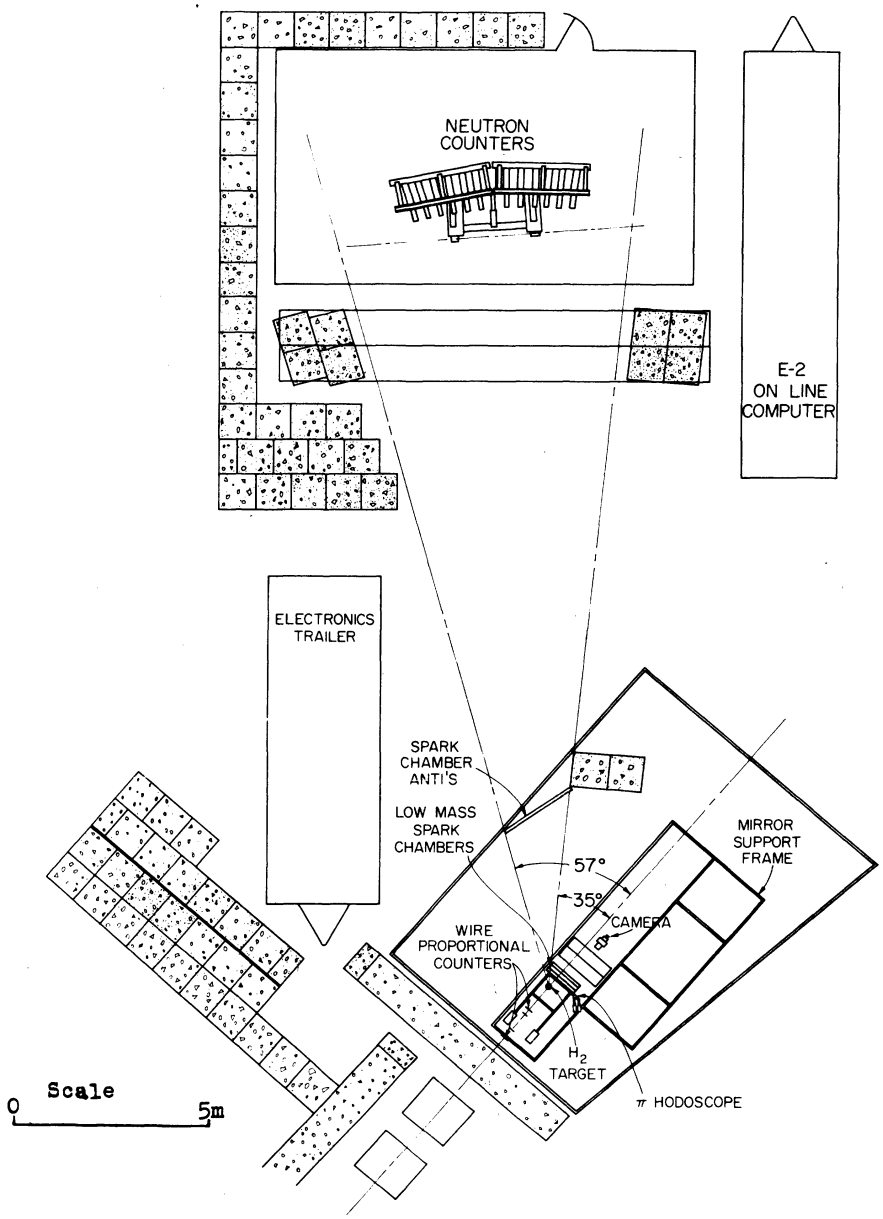

FIG. 2. Neutron flight path. The ZGS 17° beam is incident from the lower left. Recoil neutrons from interactions in the hydrogen target are detected by the neutron counters at the top. The counters labelled "spark chamber anti's" (SCA) vetoed events when a charged particle arising from secondary scattering in the spark chambers could give a false neutron signal.

neutron angles covered and the time-of-flight gate, is shown in Fig. 3.

An event signal triggered the spark chambers, camera advance circuit, and fast fiducials. An event scaler drove two parallel sets of binary lights recorded in the picture, and the event number which was recorded on magnetic tape by the Σ-2 computer. Neutron time-of-flight, pulse height, hodoscope counter and wire hits, run number (also in lights), and a flag distinguishing data events and prompts were also recorded on tape.

III. DATA REDUCTION

A separate data run at 2.5 GeV/c, looking at the ω meson, previously reported,[8] served to check the time-of-flight (and mass) resolution, and also provided a significant new measurement of the ω width. The time-of-flight resolution was found to be 0.85 ± 0.10 nanoseconds rms.

Separate runs were also taken of elastic scattering and beam tracks. These runs were useful in checking optical constants for the spark chambers. Elastic events also provided an independent measure of the magnitude of the beam momentum and its vertical divergence.

The film was measured by the University of Illinois DOLLY system.[9] Optical constants for particular sets of data were generated from on-site surveying data and fiducial measurements using a Nuclear Research Instruments (NRI) film-plane measuring device. The constants were entered into DOLLY. For each frame DOLLY searched for fiducial marks, and a least-squares fit was made to align the observed fiducials with the expected positions. To be properly registered, the rms error of the fit to five fiducials had to be less than 15 microns in the film coordinates (a magnification of $\frac{1}{60}$ was used). If, for a set of data, a significant fraction of events failed to register, new optical constants were generated for that data. DOLLY decoded the binary lights and scanned the calculated positions of the gaps, digitizing spark positions and widths. DOLLY magnetic tape output was then merged with Σ-2 information; a total of 452 000 events, corresponding to 9.52×10^{10} incident beam particles, were successfully merged.

A pattern recognition program then interpreted the spatially reconstructed sparks. The pattern program stepped through the gaps, grouping sparks. A spark either formed a new group or was added to an existing group if it was in an allowed transverse region within three gaps of another spark. The first ten gaps of the shower chambers were scanned first, and any track candidates found were projected into the foil chamber in order to search for associated sparks. The program then stepped through the remaining sparks in the foil chamber. An attempt to link groups followed. This procedure was carried out in the side view and then in the top view, using the small angle top view stereo on the foil chamber as well as missing sparks and spark intensities to match the views. Up to four final tracks were allowed. The minimum requirement for a track was two sparks in the foil chamber. Electromagnetic shower information was not used in this analysis. Further details of this program are found in Ref. 7.

A successfully reconstructed event was required to have appropriate latched counter information. Events where information was present but ambiguous were rejected if the ambiguity was in the neutron polar angle θ, the Pi hodoscope, the Momentum hodoscope, or both MWPCs (adjacent wires were accepted and averaged). Seven percent of the events failed because of improper latch information. Events were further required to yield a unique pair of tracks, corresponding to the latched Pi hodoscope elements, which successfully extrapolated to an interaction point in the target consistent with MWPC determination of the incident beam particle. An additional 29% of the events were lost by these requirements.

A kinematic fit to the 2-constraint (2C) hypothesis $\pi^- p \to \pi^+ \pi^- n$ was attempted for all successfully reconstructed events. Due to ambiguity in fits involving particles of low momentum, events in the resulting data sample were required to have pion momenta greater than 100 MeV/c. The χ^2 distribution for these fits, shown in Fig. 4, is well de-

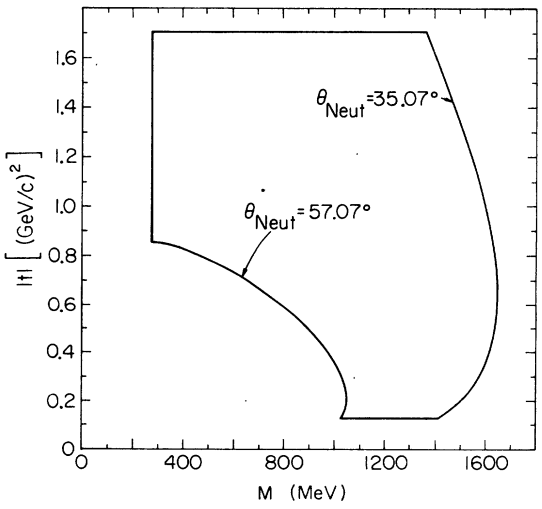

FIG. 3. Allowed region of meson mass and momentum transfer. The boundaries of the accepted region are determined by the angular range covered and the allowed neutron time-of-flight gate.

scribed by the expected distribution for a two-constraint fit plus a constant background. This χ^2 distribution corresponds to an overestimation of errors of about 14%. A total of 8661 events yielded 2C fits.

Events were weighted by the geometric acceptance implied by the polar angle of the neutron. The weight compensates for the variation of azimuthal acceptance with polar angle and the multiple coverage of central angles. Small corrections for the different amounts of beam corresponding to different neutron counter positions, details of precise spacing, and edge overlap, taking into account the angular divergence of the beam and the length of the target are included in the weight.

The acceptance of the pion arm varies with mass, momentum transfer, and the decay angles of the two-pion system. A direct calculation of acceptance for a two-pion effective mass of 1.27 GeV and momentum transfer squared $|t| = 0.3$ $(\mathrm{GeV}/c)^2$, a typical case, is shown in Fig. 5. Decay of two-pion systems in the mass and t regions of interest is known to be sharply forward peaked in polar decay angle in the Gottfried-Jackson frame ($\cos\theta_{GJ}$); acceptance is thus a strong function of the variation of this distribution with mass and momentum transfer.

A series of fiducial cuts were places on the data as follows:

1. Tracks must pass through two distinct hodoscope elements.
2. No track passing through the beam anti-counter was allowed.
3. Tracks must be separated in a direction perpendicular to the optic axis of the horizontal view by at least 2.5 cm at the center of the foil chamber.
4. The interaction vertex must be located inside the liquid hydrogen target.
5. Both tracks must pass through the active area of at least six gaps of the foil chambers.

A total of 11.1% of the data was lost by these cuts. The efficiency was then determined by subjecting Monte Carlo generated events to these cuts. Although the spot size and divergence of the beam, the length of the target, the range of allowed neutron laboratory angles, as well as a finite range of mass and momentum transfer tend to blur the boundaries of Fig. 5, regions of zero acceptance remain. The Monte Carlo events were generated isotropically in decay, and flat in t and mass. A preliminary description of the decay distribution of the form

$$W(X) = A + Bx^2 + Cx^4,$$

where $x = \cos\theta_{GJ}$, was determined for different regions of mass and t. The Monte Carlo events were then weighted according to this distribution to determine efficiency as a function of t. This efficiency varied from 48% at lowest momentum transfer to about 68% for $|t|$ above 0.8. This weight multiplied by an exponentially falling t weight was used to determine the efficiency in decay angles. The resulting (iterated) efficiency for $\cos\theta_{GJ}$ changed only slightly from the original, near $\cos\theta_{GJ} = 1$. Details of these procedures can be found in Ref. 10.

To obtain a reasonably pure sample of events, the χ^2 values of the 2C kinematic fits were required to be less than 3.5. In determining production and decay angular distributions, a region of higher χ^2 (4.5 to 8) was subtracted in order to compensate for background. The efficiency of this procedure was studied as a function of t by ran-

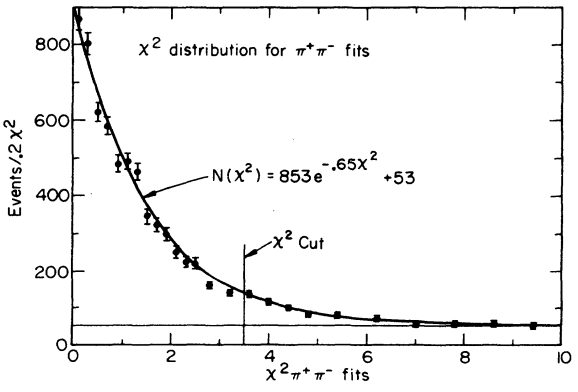

FIG. 4. Distribution in χ^2 for two-constraint kinematic fits. The form shown corresponds to a 14% overestimation of errors and a constant background.

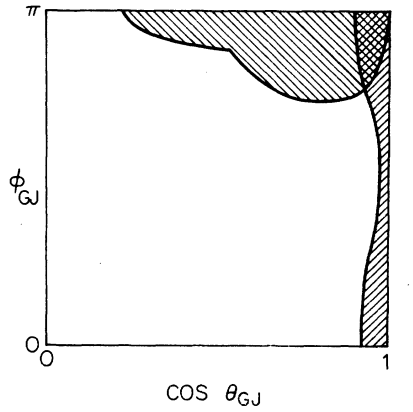

FIG. 5. Directly calculated acceptance of $(\pi^+\pi^-)$ decay angles. A mass of 1.27 GeV, $-t$ of 0.3 $(\mathrm{GeV}/c)^2$, an interaction in the center of the target, and a neutron recoiling in the horizontal plane are assumed. This is a fairly typical case. The region about $\cos\theta = 1$ is lost by the beam veto and the region about $\phi = \pi$ is lost by wide-angle tracks missing the spark chambers.

domizing fitted two pion events according to the known measurement errors and kinematically fitting the resulting "measurements." The χ^2 distribution of the resulting fits shows that the efficiency of the subtraction (for good events) varies from 86% at the lowest $|t|$ to 82% at the highest accepted $|t|$. In the differential cross sections quoted this efficiency has been taken into account. The differential cross sections have also been corrected for neutron scattering losses and neutron counter efficiency (~28%), as determined by the Kurz program.[11] Neutron counter efficiencies vary by only 6.7% over the range of neutron kinetic energies covered (67–900 MeV).

IV. RESULTS AND CONCLUSIONS

Events passing the two-constraint hypothesis of the $\pi^+\pi^-$ fits in the momentum transfer interval $0.15 < |t| < 0.5$ $(\mathrm{GeV}/c)^2$ are shown in Fig. 6. Events have been weighted only for neutron acceptance. The data were binned in 10-MeV intervals outside the f^0 peak region (1185–1355 MeV) and in 5-MeV bins in the peak region. The mass resolution, also shown, was obtained by adding the Gaussian resolution functions for each event in the sample, and has a value of 8 MeV FWHM. The figure shows the best Breit-Wigner and dipole fits obtained by folding in the mass resolution and employing a linear background. The narrow available mass range and the inadequacy of a linear background preclude a determination of the f^0 mass and width. The widths of the curves were constrained in the fitting by adding a contribution to χ^2 of the form $[(\Gamma_{\mathrm{fit}} - \Gamma_{\mathrm{input}})/\Delta\Gamma_{\mathrm{input}}]^2$, where Γ_{input} is inserted as 156 ± 25 and 60 ± 40 MeV for the Breit-Wigner and dipole, respectively.[12] The χ^2's of the Breit-Wigner and dipole fits are 39.9 and 71.5, respectively, for 54 degrees of freedom, corresponding to confidence levels of 92.1% and 5.4%.

A quantity that has been used[13] as a measure of possible structure in the A_2 mass spectrum is the duplicity parameter δ, the mass spectrum being

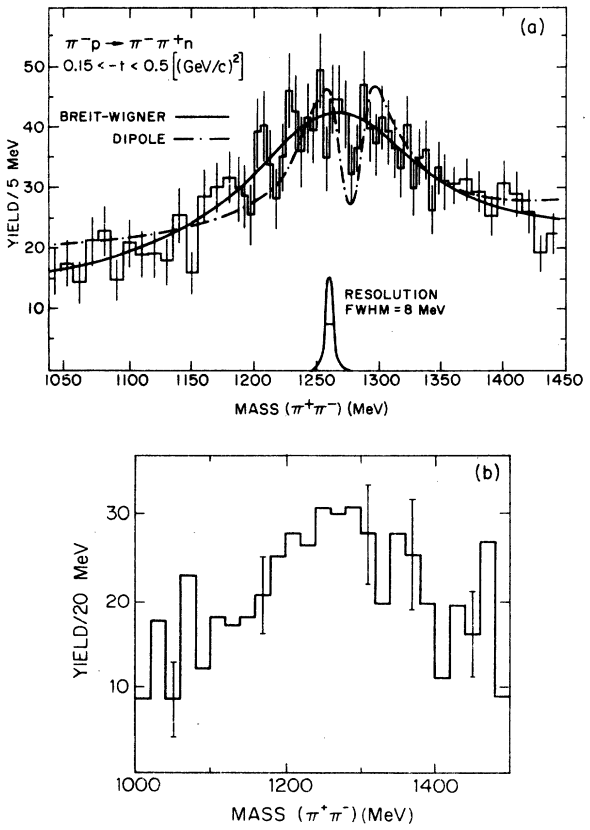

FIG. 6. Neutron acceptance weighted $(\pi^+\pi^-)$ mass spectra, (a) $0.15 < |t| < 0.5$ $(\mathrm{GeV}/c)^2$ showing simple Breit-Wigner and dipole fits, and (b) $0.8 < |t| < 1.4$.

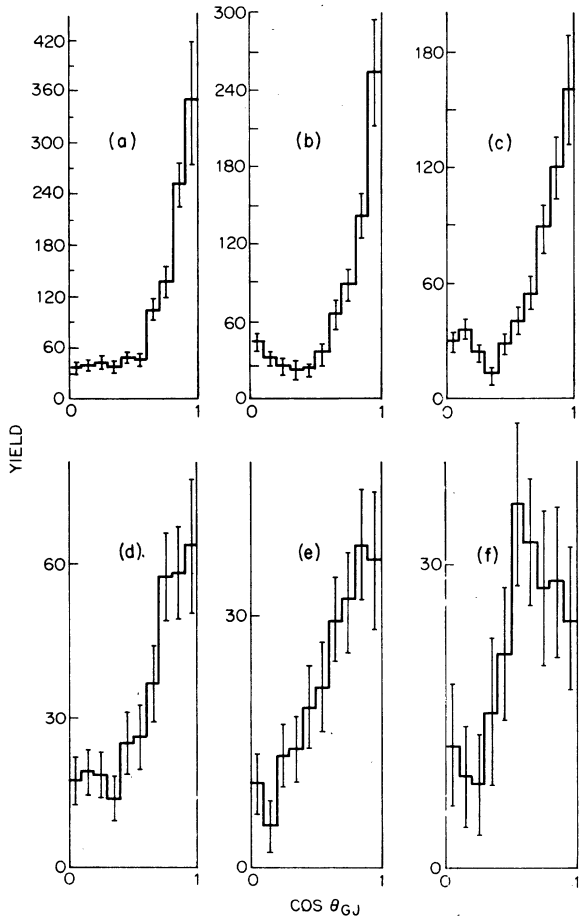

FIG. 7. f^0 region distributions in $\cos\theta_{GJ}$ for intervals of momentum transfer squared $[-t$, in $(\mathrm{GeV}/c)^2]$ (a) 0.125 – 012, (b) 0.2 – 0.3, (c) 0.3 – 0.5, (d) 0.5 – 0.85, (e) 0.85 – 1.1, (f) 1.1 – 1.6.

fitted to the combination

$$F(M) = \delta \times \text{dipole} + (1-\delta) \times \text{Breit-Wigner} + \text{background}.$$

In fits with a combination of dipole and Breit-Wigner terms, it is necessary to constrain the dipole width; if unconstrained, a too narrow width allows for accommodation of bin-to-bin fluctuations. Therefore, we used a width $\Gamma = 38 \pm 4$ MeV, the value obtained in the best dipole fit. The Breit-Wigner width was constrained as noted earlier. We obtained a duplicity parameter

$$\delta_{f0} = -0.04 \pm 0.08,$$

a result clearly consistent with zero.

Figure 6(b) shows the same distribution for $0.8 \leq |t| \leq 1.4$ (GeV/c)^2, with a strong f^0 signal still present.

The distributions in $\cos\theta_{GJ}$ of two-pion events in the f^0 region (1170–1370 MeV) are shown for different regions of momentum transfer in Fig. 7. These and succeeding distributions have been fully compensated for acceptances. Since our apparatus is not sensitive to the sign of the charge of the outgoing pions, we only define $\cos\theta_{GJ}$ between 0 and 1, and the azimuthal decay angle ϕ_{GJ} between 0 and π. The sharp forward peak expected for f^0's is seen to diminish for higher momentum transfer. We parametrize the decay angular distribution as the spin-density matrix elements for spin-2 decay, fitting the distributions to

$$W(\theta) = \tfrac{15}{8}[\rho_{00}(3\cos^2\theta - 1)^2 + 4\rho_{11}\cos^2\theta \sin^2\theta + \rho_{22}\sin^4\theta],$$

$$W(\phi) = \frac{1}{2\pi}\{1 - 2[\rho_{1-1} + (\tfrac{2}{3})^{1/2}\mathrm{Re}\rho_{20}]\cos 2\phi + 2\rho_{2-2}\cos 4\phi\}.$$

The resulting density-matrix elements are shown in Fig. 8. The values in the helicity frame as well as the Gottfried-Jackson frame, are listed in Table I. They agree well with the previous results for low momentum transfer. The large value of ρ_{00} (Gottfried-Jackson) is characteristic of simple OPE. The negative value of ρ_{22} can be attributed to interference with a spin-zero dipion state, possibly resonant.[14] The primary effect of such a $J^P = 0^+$ two-pion state is an interference term in the decay distribution proportional to $P_2(\cos\theta_{GJ})$. If such a term is large enough to decrease the value of ρ_{22} by 0.2, it would raise the value of ρ_{00} by about 0.03; the unnatural-parity fraction would be overestimated by about 0.02.

The rapid falloff of ρ_{00} and the increasing importance of off-diagonal elements at high momentum transfer is apparent. It is illuminating to compute the total unnatural-parity-exchange fraction, which is given in the Regge limit by[15]

$$f_u = \tfrac{1}{2} + \tfrac{1}{2}\rho_{00} - \rho_{1-1} + \rho_{2-2}.$$

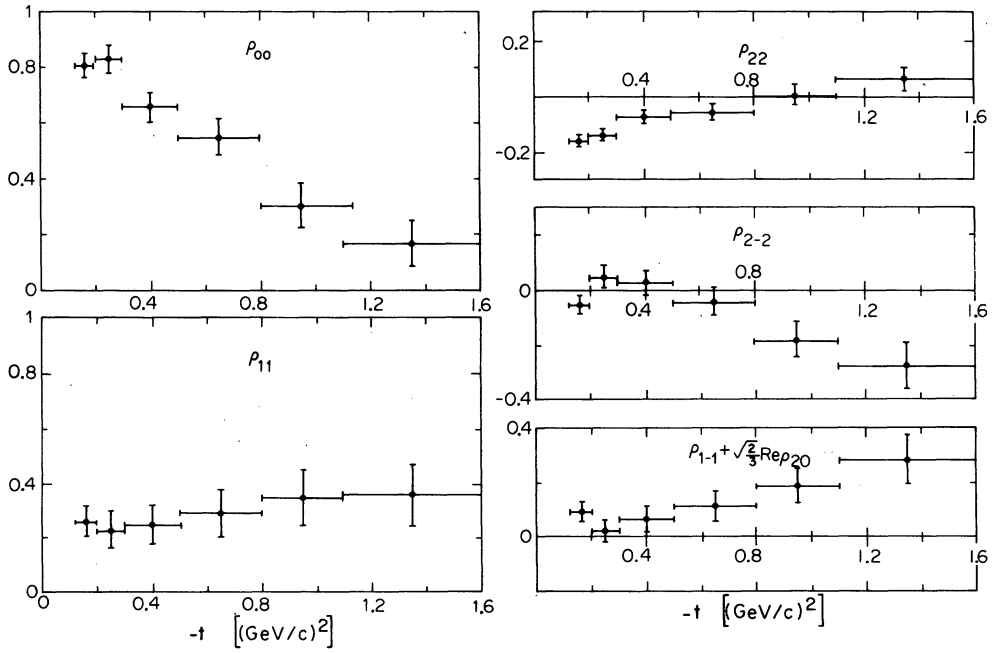

FIG. 8. Spin-2 decay spin-density matrix elements for the f^0 region in the Gottfried-Jackson frame.

TABLE I. Density-matrix elements and unnatural-parity fraction.

$-t$	ρ_{00}		ρ_{22}		$\rho_{1-1}+(\frac{2}{3})^{1/2}\mathrm{Re}\rho_{20}$		ρ_{2-2}		
[(GeV/c)^2]	GJ	Helicity	GJ	Helicity	GJ	Helicity	GJ	Helicity	f_u
0.125–0.2	0.808 ± 0.042	0.586 ± 0.074	− 0.162 ± 0.017	− 0.123 ± 0.027	0.092 ± 0.035	− 0.109 ± 0.034	− 0.− 49 ± 0.035	− 0.082 ± 0.034	0.763 ± 0.054
0.2–0.3	0.830 ± 0.051	0.298 ± 0.130	− 0.142 ± 0.023	− 0.009 ± 0.049	0.020 ± 0.044	− 0.223 ± 0.039	0.048 ± 0.041	− 0.032 ± 0.041	0.943 ± 0.065
0.3–0.5	0.656 ± 0.056	0.330 ± 0.102	− 0.076 ± 0.025	0.026 ± 0.041	0.065 ± 0.046	− 0.186 ± 0.040	0.028 ± 0.044	− 0.078 ± 0.042	0.791 ± 0.070
0.5–0.8	0.546 ± 0.069	0.060 ± 0.085	− 0.060 ± 0.028	0.215 ± 0.039	0.114 ± 0.057	− 0.249 ± 0.047	− 0.042 ± 0.051	− 0.076 ± 0.049	0.617 ± 0.084
0.8–1.1	0.299 ± 0.079	0.032 ± 0.116	0.005 ± 0.035	0.290 ± 0.054	0.191 ± 0.064	− 0.161 ± 0.058	− 0.178 ± 0.062	− 0.167 ± 0.064	0.280 ± 0.097
1.1–1.6	0.164 ± 0.081	0.110 ± 0.102	0.061 ± 0.040	0.256 ± 0.056	0.286 ± 0.089	0.021 ± 0.071	− 0.269 ± 0.080	− 0.267 ± 0.070	0.027 ± 0.126

In order to separate ρ_{1-1} and $\mathrm{Re}\rho_{20}$, we fit our observed distribution to

$$W(\theta,\phi)=\frac{15}{16\pi}[(\rho_{22}+\rho_{2-2}\cos4\phi)\sin^4\theta + 4(\rho_{11}-\rho_{1-1}\cos2\phi)\sin^2\theta\cos^2\theta + \tfrac{1}{3}\rho_{00}(3\cos^2\theta-1)^2 + 2(\tfrac{2}{3})^{1/2}\mathrm{Re}\rho_{20}\cos2\phi\sin^2\theta(3\cos^2\theta-1)].$$

Our apparatus is not sensitive to odd terms. We find $\mathrm{Re}\rho_{20}$ very small (approximately 0.04) and not varying with t, and we therefore feel justified in taking $\rho_{1-1}\approx\rho_{1-1}+(\frac{2}{3})^{1/2}\mathrm{Re}\rho_{20}$. The result is shown in Fig. 9.

Unnatural parity exchange (presumably pion exchange) is no longer dominant for $|t|$ above ~0.7 (GeV/c)^2, and, at high momentum transfer, natural parity exchange dominates the cross section. A similar crossover was recently observed in ρ-meson production in the analysis of Grayer *et al.*[16] The crossover observed in their 17-GeV/c data is at $|t|\sim0.3$ (GeV/c)^2.

The differential cross section is shown in Fig. 10. Also shown are cross sections for low (1050–1170 MeV) and high (1370–1490 MeV) mass regions, and for the ρ region (700–860 MeV) which is accepted at high momentum transfer. The various cross sections are normalized relative to each other. We observe that the shape of the differential cross section is not perceptibly a function of $(\pi^+\pi^-)$ mass in the accepted region (1050–1490 MeV). The gradual falloff for the ρ region at large momentum transfer suggests a similar shape.

The drawn curve corresponds to a calculation from Wolf's one-pion-exchange model, using parameters from Wolf's fit[3] normalized to our data

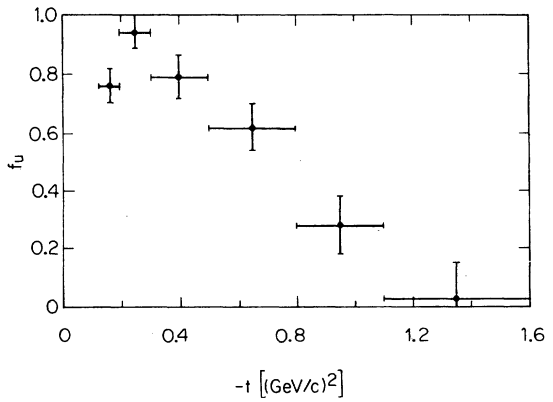

FIG. 9. Unnatural-parity-exchange fraction for the f^0 region.

TABLE II. Differential cross section $d\sigma/dt$ for $\pi^- p \to \pi^+ \pi^- n$, $1170 < M(\pi^+\pi^-) < 1370$ GeV, normalized at lowest $|t|$ to a Wolf-model f^0 cross section of 400 μb.

$-t$ [(GeV/c)^2]	$d\sigma/dt$ [μb/(GeV/c)^2]	$-t$ [(GeV/c)^2]	$d\sigma/dt$ [μb/(GeV/c)^2]
0.125 – 0.15	1150 ± 89	0.5 – 0.6	81.9 ± 9.3
0.15 – 0.175	891 ± 72	0.6 – 0.7	66.5 ± 8.3
0.175 – 0.2	767 ± 65	0.7 – 0.85	59.6 ± 5.4
0.2 – 0.25	528 ± 39	0.85 – 1.0	41.3 ± 4.7
0.25 – 0.3	353 ± 31	1.0 – 1.2	46.0 ± 4.6
0.3 – 0.35	267 ± 25	1.2 – 1.4	26.2 ± 4.1
0.35 – 0.4	193 ± 22	1.4 – 1.6	16.5 ± 4.0
0.4 – 0.5	138.7 ± 12.7		

at lower $|t|$. The Wolf model curve agrees well with the observed cross section for momentum transfers less than $|t| \approx 0.7$ (GeV/c)^2. The cross section for large momentum transfer is greater than predicted by the model. Values of the f^0-region differential cross section are listed in Table II.

In summary, we find no evidence for fine structure in the dipion mass spectrum in the region of the f^0. We find an unexpectedly high differential cross section at large momentum transfer, dominated by natural parity exchange.

We would like to thank the ZGS staff, and Argonne National Laboratory for the use of the neutron-counter hodoscope and the Σ-2 computer. We also wish to thank R. M. Brown and J. Wray for their work on DOLLY programming, and to thank G. Ascoli for useful discussions and aid in the analysis.

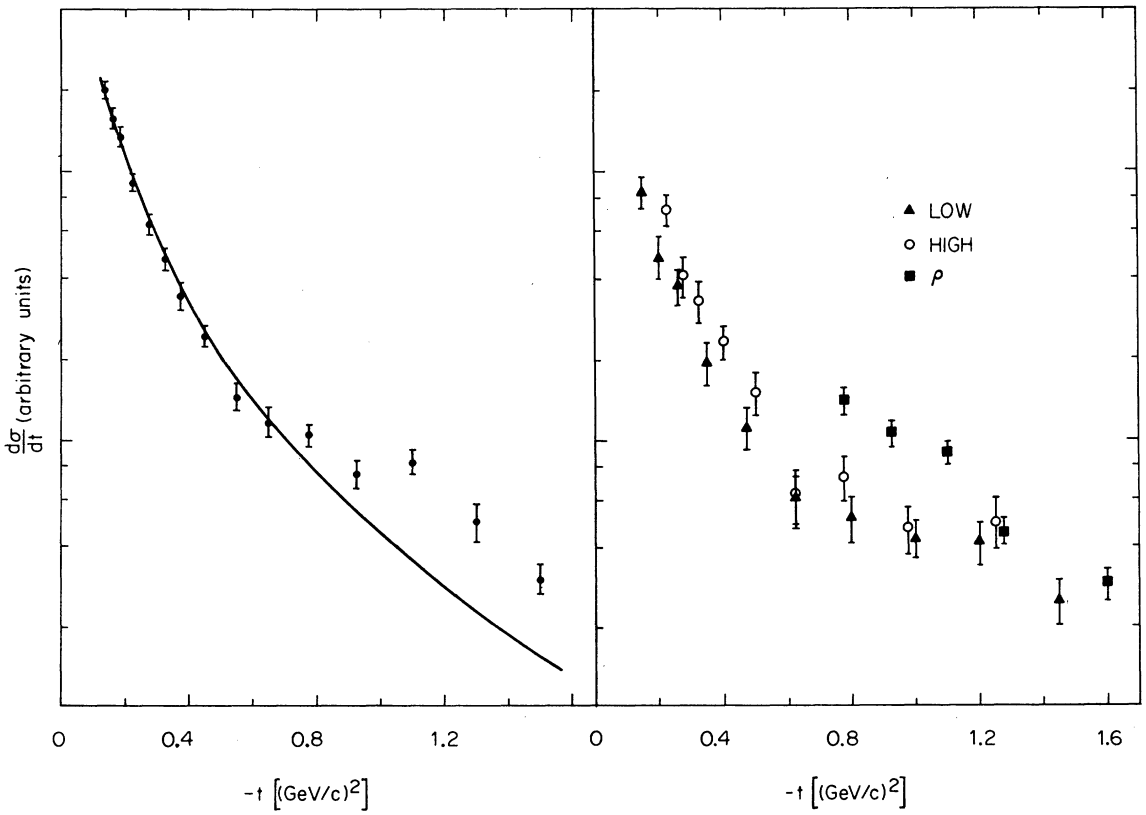

FIG. 10. Differential cross section, $d\sigma/dt$, for the f^0 region (117–1310 MeV), and for high (1370–1490), low (1050–1170), and ρ-meson (700–860 MeV) regions.

*Work supported in part by the U. S. Atomic Energy Commission.

†Present address: 15 Alpine Street, Cambridge, Massachusetts 02139.

‡Present address: Department of Physics, Northeastern University, Boston, Massachusetts 02115.

§Present address: DESY, Hamburg-Gr-Flottbek, Notkestieg 1, Germany.

‖Present address: Telemed, 9950 West Lawrence, Shiller Park, Illinois 60176.

[1]Splitting of the f^0 mass spectrum was reported by P. H. Stuntebeck, V. P. Kenney, B. J. Deery, N. N. Biswas, N. M. Cason, A. R. Dzierba, M. S. Farber, J. A. Poirier, and W. D. Shephard, Phys. Lett. 32B, 391 (1970); D. Kemp, J. V. Major, S. M. Scarriott, R. Contri, D. Teodoro, G. Tomasini, E. Calligarich, S. Ratti, G. Vegni, G. DeRosny, J. Huc, R. Sosnowski, J. M. Terreault, M. Barrier, H. K. Nguyen, and J. Quinquard, Nuovo Cimento 8A, 611 (1972). A nonsplit f^0 was reported by S. A. Flatté, M. Alston-Garnjost, A. Barbaro-Galtieri, S. E. Derenzo, J. H. Friedman, G. R. Lynch, S. D. Protopopescu, M. S. Rabin, and F. T. Solmitz, Phys. Lett. 34B, 551 (1971).

[2]Previous f^0 studies include J. A. Poirier, N. N. Biswas, N. M. Cason, I. Derado, V. P. Kenney, W. D. Shephard, E. H. Synn, H. Yuta, W. Selove, R. Ehrlich, A. L. Baker, Phys. Rev. 163, 1462 (1967); M. S. Farber, J. V. DePinto, N. N. Biswas, N. M. Cason, B. J. Deery, V. P. Kenney, J. A. Poirier, O. R. Sander, and W. D. Shephard, Nucl. Phys. B29, 237 (1971); M. T. Fogli-Muciaccia and V. Picciarelli, Nuovo Cimento 8A, 670 (1972).

[3]G. Wolf, Phys. Rev. 182, 1538 (1969).

[4]L. E. Holloway, G. Huld, M. Jordan, D. W. Mortara, E. I. Rosenberg, A. D. Russell, S. Bernstein, M. H. Garrell, S. Margulies, and D. W. McLeod, Phys. Rev. D 8, 2814 (1973).

[5]L. J. Koester, U. Koetz, and S. Segler, Nucl. Instrum. Methods 82, 67 (1970).

[6]G. L. Schnurmacher, A. R. Clark, and L. T. Kerth, Nucl. Instrum. Methods 61, 89 (1968).

[7]M. Jordan, thesis, University of Illinois, Urbana, 1972 (unpublished).

[8]R. M. Brown, R. W. Downing, L. E. Holloway, B. Huld, M. Jordan, U. Koetz, U. E. Kruse, D. W. Mortara, L. J. Nodulman, V. J. Simaitis, J. J. Wray, D. R. Zander, S. Bernstein, S. Margulies, and D. W. McLeod, Phys. Lett. 42B, 117 (1972).

[9]R. M. Brown and R. W. Downing, Proceedings of the International Conference on Advanced Data Processing for Bubble and Spark Chambers, available as Argonne National Laboratory Report No. ANL-7515, 1968 (unpublished).

[10]L. J. Nodulman, thesis, University of Illinois, Urbana, 1973 (unpublished).

[11]R. J. Kurz, LBL Report No. UCAL-11339, 1964 (unpublished).

[12]The Breit-Wigner width was constrained as listed by the Particle Data Group, Phys. Lett. 39B, 1 (1972). The dipole width was loosely constrained to overlap previously obtained values.

[13]G. Lynch, LBL Report No. UCRL 26022, 1971 (unpublished).

[14]J. V. Beaupré, M. Deutschmann, H. Graessler, P. Schmitz, R. Speth, H. Boettcher, J. Katwasser, H. Kaufmann, S. Nowak, A. Angelopoulos, K. W. J. Barnham, J. R. Campbell, V. T. Cocconi, P. F. Dalpiaz, J. D. Hansen, G. Kellner, W. Kittel, and D. R. O. Morrison, Nucl. Phys. B28, 77 (1971); and C. Whitehead, D. West, L. Bird, E. G. Auld, D. G. Crabb, R. Ott, J. G. McEwen, D. K. Aitken, G. Bennett, J. F. Hague, R. E. Jennings, and A. S. L. Parsons, Nucl. Phys. B48, 365 (1972).

[15]J. P. Ader, M. Capdeville, G. Cohen-Tannoudji, and P. Salin, Nuovo Cimento 56A, 952 (1965).

[16]G. Grayer, B. Hyams, C. Jones, P. Weilhammer, W. Blum, H. Dietl, W. Koch, E. Lorenz, G. Lütjens, W. Männer, J. Meissburger, W. Ochs, and U. Stierlin, Nucl. Phys. B50, 29 (1972).